Preparation of a Porous Structure in a Poly(4-Methyl-1-Pentene)/Diphenyl Ether System with a Thermally Induced Phase-Separation Method

Qiang Zhang,[1,2] Youquan Zhang,[3] Dewan Xia,[1,2] Yun Zhao,[2] Yanqiao Shi,[1] Qingze Jiao[2]

[1]*Institute of Chemistry, Chinese Academy of Sciences, Beijing 100080, People's Republic of China*
[2]*School of Chemical Engineering and Environment, Beijing Institute of Technology, Beijing 100081, People's Republic of China*
[3]*School of Chemistry and Chemical Engineering of Guangxi University, Nanning 530004, People's Republic of China*

Received 20 June 2007; accepted 28 September 2008
DOI 10.1002/app.29458
Published online 30 January 2009 in Wiley InterScience (www.interscience.wiley.com).

ABSTRACT: Poly(4-methyl-1-pentene) was used to prepare porous structures by a thermally induced phase-separation method. Different porous structures were obtained with poly(4-methyl-1-pentene), which has excellent properties as a polymer, and diphenyl ether as a diluent. The affecting factors, including the polymer concentration and cooling temperature, are discussed. Scanning electron microscopy images and porosity values were obtained to investigate the affecting factors. According to the cloud-point temperature and crystallization temperature, a phase diagram was also obtained to explain the phase-separation process. © 2009 Wiley Periodicals, Inc. J Appl Polym Sci 112: 1271–1277, 2009

Key words: microstructure; phase diagrams; phase separation

INTRODUCTION

Poly(4-methyl-1-pentene) (TPX) is a common crystalline polymer, which has a high melting temperature (227°C) and excellent mechanical properties. TPX has been widely used in industry and in medical products and has a potentially wide range of applications because of its excellent optical clarity, higher melting temperature, electrical properties, low bulk density, high chemical resistance, and high permeability to gases.[1,2]

Its mechanical properties are comparable to other polyolefins at room temperature, with a melting temperature that is higher than that of common polyolefins, such as polyethylene and polypropylene. These intrinsically desirable characteristics have led to many studies of the structure and properties of this polymer.[3–9] TPX's good electrical properties and heat resistance have been investigated for applications in heat-resistant wire, power, oil wells, and communication cables.[10] It has also been used in labware and medical products, such as blood testing and medical instruments and syringes.[11] Rosa and coworkers[12–15] studied the crystal structure of TPX. Pande et al.[16] studied normal modes and their dispersion for TPX. The structure of TPX is shown in Figure 1.

Nowadays, porous membranes have been widely applied in variant fields, including in the food industry, oil–water separation, and water and wastewater treatment. Particularly, porous membranes are mainly used for aqueous separation.[17] Normally, TPX membranes are made by the immersion–precipitation method, dry method, and so on.[18–24] However, we used thermally induced phase separation (TIPS) to fabricate the TPX porous structures in this particular study. The TIPS method was first described in U.S. patent 4,247,498 by Anthony J. Castro.[25] The TIPS process changes the thermal energy to induce the demixing of a homogeneous polymer/diluent solution either by solid–liquid (S–L) demixing or liquid–liquid (L–L) phase separation. In the case of an L–L phase-separation mechanism, two definitively different morphologies may be produced: (1) the solution separates into polymer-rich and polymer-lean phases when cooled below the binodal curve, or (2) the solution separates into a bicontinuous polymer-rich and polymer-lean phases when cooled below the spinodal curve. The second process makes it easier to form a highly interconnected polymer network after the dilute is extracted. The most attractive characteristics are not only the intrinsically interconnected polymer network that can be formed but also the speed and controllability of the process through the TIPS

Correspondence to: D. Xia (xiadewan@163.com).
Contract grant sponsor: National Basic Research Program of China; contract grant number: 2003CB615701.

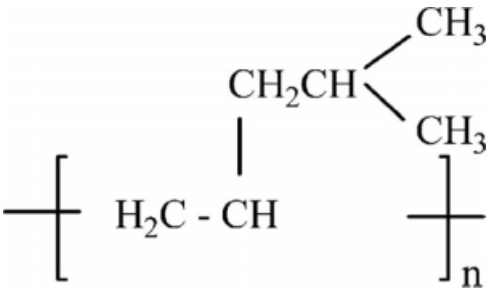

Figure 1 Structure of TPX.

method. Thus, TIPS is a very convenient technique for the fabrication of porous membranes, as many membrane structures can be formed with ease via the manipulation of various processing parameters and system properties.[26]

Some groups have investigated the phase-separation mechanism and affecting factors of microporous membrane formation by the TIPS method, and many different materials have been used.[27–46] However, TPX has seldom been used so far to prepare the membrane by the TIPS method.

To prepare porous TPX membranes with various pore structures via the TIPS method, we chose diphenyl ether (DPE) as a new diluent. The phase diagram and the affecting factors, including the concentration of TPX and different cooling rates, on the porous structure were examined.

EXPERIMENTAL

Materials

Poly(4-methyl-l-pentene) was a commercial product of Mitsui Petrochemicals Industries., Ltd. (Chiyoda-Ku, Tokyo, Japan) under the commercial name of TPX type MX-004 and had a melt flow index of 25 g/10 min. DPE (analytical-reagent grade, melting temperature = 26°C, boiling point temperature = 256°C) was commercial product of Beijing Chemical Factory. Both acetone (analytical-reagent grade) and ethanol (guaranteed reagent) were commercial products of Beijing Chemical Factory.

Membrane preparation

The steps for preparing the porous TPX samples are described next. First, the TPX and the diluent (DPE) were put into a test tube and mixed at special weight ratios, and then, the test tube was filled with nitrogen and sealed with a stopper with aluminum leaf. The test tube was put into an electric heating apparatus and heated to 10–20°C below the boiling point of the diluent until the TPX was dissolved completely in the diluent. Last, the test tube was put suddenly into cooling media (air or water) or cooled slowly (10°C/min) to solidify.

The diluent in the example was extracted by acetone, and then, the sample was dried in a vacuum drying oven at 60°C for 24 h.

Phase diagrams

All of the phase diagrams showed upper critical solvent temperature (UCST) type L–L phase behavior. Because TPX is a crystalline polymer, the L–L phase boundary intersected with the dynamic crystallization curve at the monotectic point. The cloud point (L–L phase separation) was observed by optical microscopy. The steps were as follows. The TPX/diluent samples were first sealed in two slides and then were heated on a hot stage to form a homogeneous solution. When the solution was slowly cooled to the cloud point, at which phase separation occurred, the transparent solution turned turbid.

The dynamic crystallization temperature was determined by differential scanning calorimetry experiment according to the following steps. A 2–4-mg sample was sealed in an aluminum differential scanning calorimetry pan, melted, usually at the endothermic peak for 3–5 min, and then cooled at 20 K/min in a PerkinElmer DSC-7. The onset of the exothermic peak during cooling was taken as the dynamic crystallization temperature.

Scanning electron microscopy (SEM) observation

The microporous samples were fractured in liquid nitrogen and mounted vertically on sample holders. The surfaces of the samples were sputtered with Au/Pd *in vacuo*. A scanning electron microscope (S-4300, Hitachi Co., Tokyo, Japan) with an accelerating voltage of 25 kV was used to observe the porous structures.

Membrane porosity

Membrane porosity is defined as the volume of the pores divided by the total volume of the porous membrane. The dry membrane was soaked in the pure ethanol for 10 h and then was taken out; the ethanol on the surface of the membrane was softly and quickly wiped up with filter paper. Finally, the membrane was weighed quickly. The formula for membrane porosity that we used was as follows:

$$\text{Membrane porosity} = \frac{(W_0 - W)\rho_1}{\rho_1 W_0 + (\rho_2 - \rho_1)W} \times 100\%$$

where W is the total weight of the dry membrane, W_0 is the weight of the wet membrane, ρ_1 is the TPX density, and ρ_2 is the absolute ethanol density.

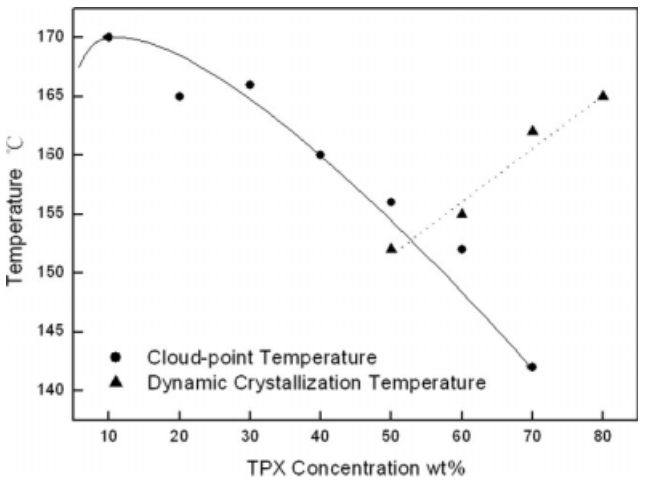

Figure 2 Phase diagram of the TPX/DPE system.

RESULTS AND DISCUSSION

Phase diagram

Figure 2 shows a phase diagram for the TPX/DPE system. When the TPX concentration was larger than 10%, as the TPX concentration increased, the cloud-point curve descended. UCST (the highest point in the cloud-point curve) was 170°C (Fig. 2). The polymer/DPE system needed to be heated above the UCST to become a homogeneous solution. The monotectic point was at the intersection of the binodal curve (or cloud-point curve) and the dynamic crystallization curve (54 wt %, 153°C). When the TPX concentration was larger than 54%, the porous structure was formed by polymer crystallization. When the TPX concentration was less than 54%, the porous structure was formed by L–L phase separation. Because the larger pore structure was formed by L–L phase separation, to obtain a TPX porous membrane with a larger pore structure, the concentration of polymer solution needed to be less than that of the monotectic point.

Effect of the TPX concentration

According to a thermodynamic consideration of the L–L phase separation, one of the most important factors affecting the pore structure is the polymer concentration. Figure 3 shows the SEM micrographs of the porous samples with different polymer concentrations under the same cooling conditions (cooled at 20°C in air). When the polymer concentrations were lower than that of the monotectic point (54 wt %), L–L phase separation played the leading role, and different pore structures were formed.

When the concentrations was 20%, a cellular morphology characteristic of L–L phase separation was formed [Fig. 3(a)].[47] When the polymer concentration was 30%, the branchlike pore structure originated from the spinodal decomposition of the L–L phase separation [Fig. 3(b)]. After the L–L phase separation, the poly-rich phase solidified to a branchlike

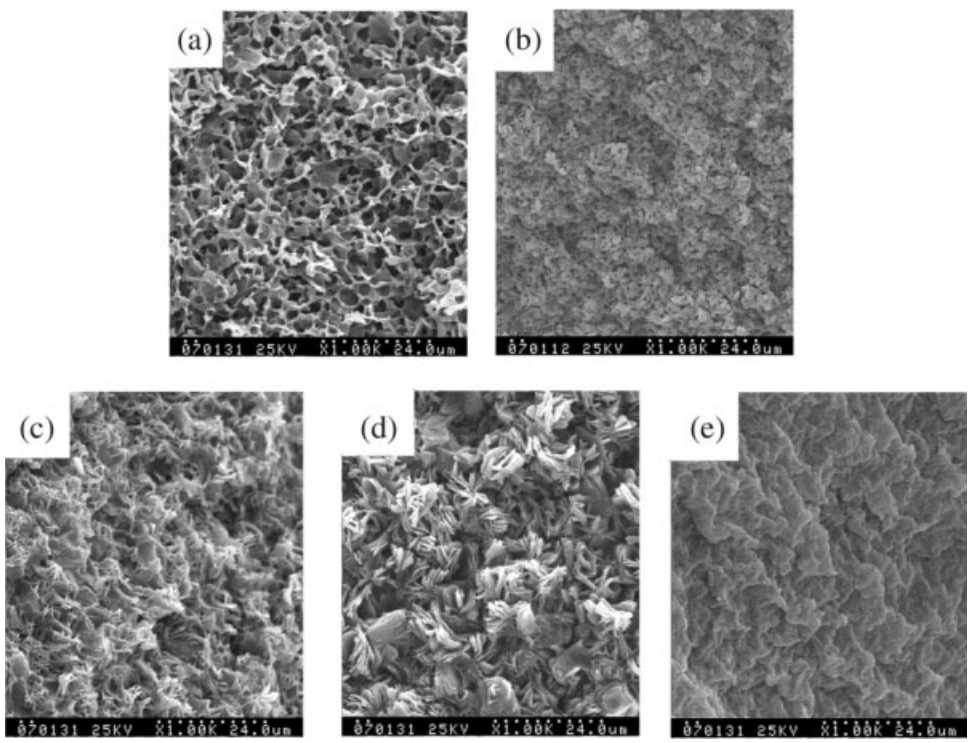

Figure 3 SEM micrographs of cross sections of TPX membranes with different concentrations quenched in 20°C air: (a) 20, (b) 30, (c) 40, (d) 50, and (e) 60 wt % (×1000).

TABLE I
Porosity at Different Concentrations with Quenching in 20°C Air

Concentration of TPX (wt %)	Porosity (%)
20	73.6
30	59.4
40	55.3
50	38.3
60	11.8

structure. Some large spherical structures were observed, as shown in Figure 3(c,d), especially in Figure 3(d). Inside the spherical structures, there were many cavities. They looked like many leaves stacked together. Hiatt et al.[48] fabricated a similar structure with poly(vinylidene fluoride). By consideration of the thermodynamic phase diagram, one can see that this kind of pore structure could be formed by two mechanisms: nucleation–growth of the polymer-rich phase in the L–L phase-separation process and crystallization of the polymer in the polymer-rich phase. In the process of pore formation, the polymer crystallization played the leading role because the solution concentration was near the concentration of the monotectic point (Fig. 2). This presented the same rule as the polyphenylene sulfide (PPS)/diphenyl ketone system.[28] However, the characteristics of the porous structure of the TPX/DPE system [Fig. 3(d)] were different from those of the PPS/diphenyl ketone system. One of the most important reasons is that many isobutyls of the TPX main chain influenced its arrangement and formation in this special structure.

The smallest pore structure is presented in Figure 3(e). This was because the polymer concentration of this solution was larger than that of the monotectic point; the S–L phase separation played a leading role. Normally, the connectivity of this kind of pore structure is poor and can be formed near the monotectic point.

Table I shows the porosity of these porous samples with different polymer concentrations under the same cooling conditions (cooled in 20°C air). Obviously, when the concentration of TPX was 20%, the porosity was highest; then, the porosity decreased with increasing TPX concentration. The SEM micrographs supported this idea (Fig. 3).When the L–L phase separation played the main role, the porosity was higher.

Figure 4 presents the SEM micrographs of the porous samples with different polymer concentrations under the same cooling conditions (quenched in 20°C water). These micrographs clearly show that both the pore density and the average pore diameter decreased when the polymer concentration increased. This was easy to elucidate by thermodynamics (Fig. 2). Figure 4(a,b) shows the typical cellular

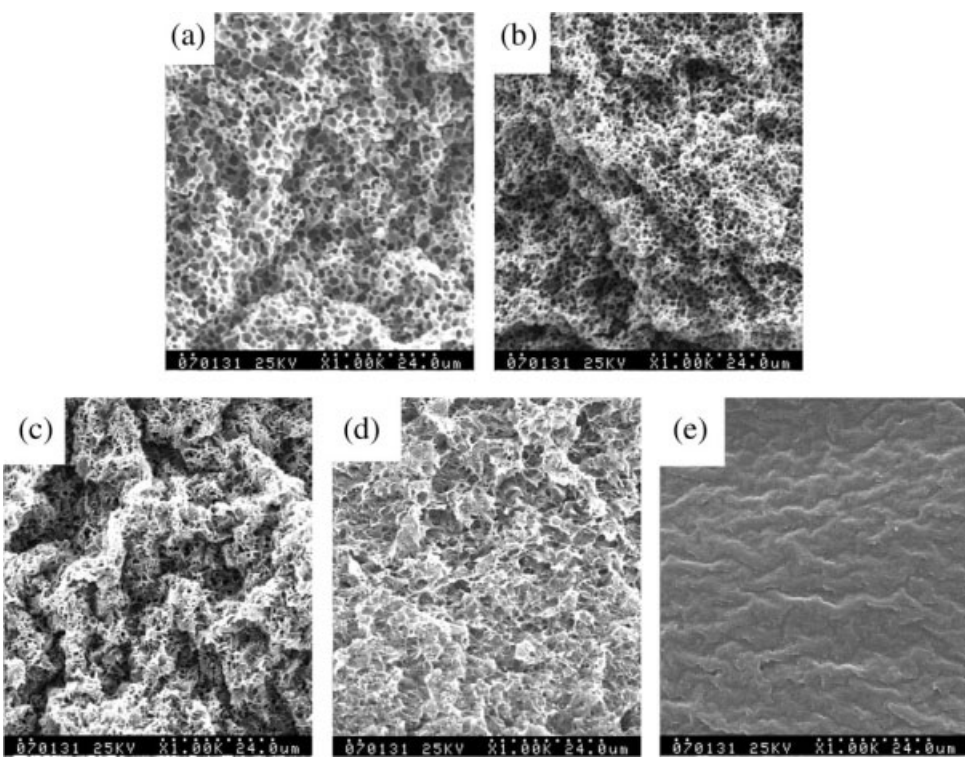

Figure 4 SEM micrographs of cross sections of TPX membranes with different concentrations quenched in 20°C water: (a) 20, (b) 30, (c) 40, (d) 50, and (e) 60 wt % (×1000).

TABLE II
Porosity at Different Concentrations with Quenching in 20°C Water

Concentration of TPX (wt %)	Porosity (%)
20	59.1
30	41.1
40	33.0
50	19.1
60	9.9

morphology. The mechanism of the formation of this structure was the same as shown in Figure 3(a). Although the pore structures shown in Figure 4(c,d) were not cellular morphology as in Figure 4(a,b), the transconnections were better than those shown Figure 4(a,b) and the permeability of the membrane was better.

Table II shows the porosity of these porous samples with different polymer concentrations under the same cooling conditions (quenched in 20°C water). Obviously, the porosities decreased with increasing TPX concentration.

As a rough rule, when the polymer concentration increased, the phase transition mechanisms in the TIPS process transformed from L–L phase separation to polymer crystallization (S–L phase separation). All the characteristics of the porous structure could be explained by the two mechanisms. The pore formation of the L–L phase separation mainly originated from two mechanisms, the nucleation–growth and spinodal decomposition mechanisms.

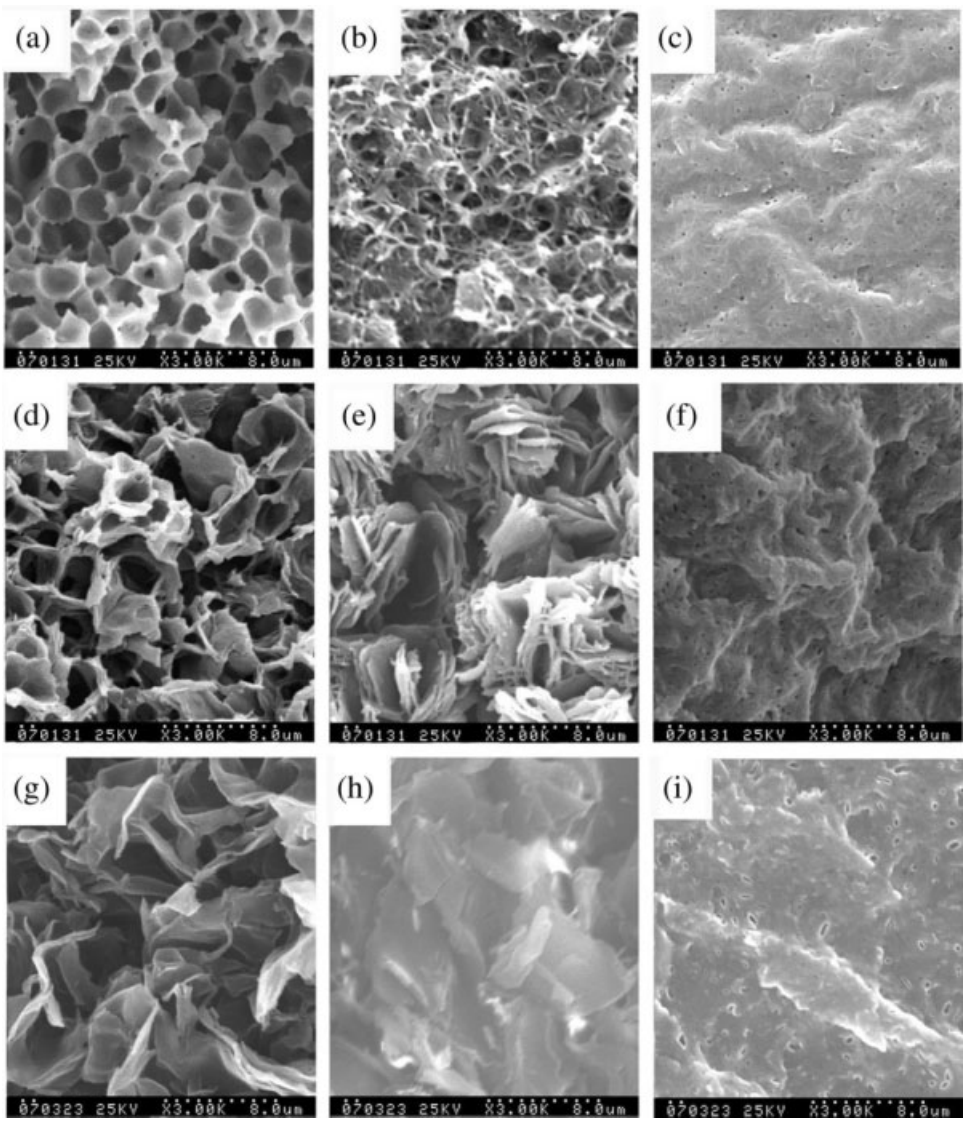

Figure 5 SEM micrographs of cross sections of TPX membranes with different concentrations (20%, 50%, and 60%) and at different cooling rates: (a) 20% and quenched in 20°C water, (b) 50% and quenched in 20°C water, (c) 60% and quenched in 20°C water, (d) 20% and quenched in 20°C air, (e) 50% and quenched in 20°C air, (f) 60% and quenched in 20°C air, (g) 20% and 10°C/min, (h) 50% and 10°C/min, and (i) 60% and 10°C/min (×3000).

Effect of the cooling rate

The driving force of phase separation in the TIPS process comes from the cooling process. When the cooling rate increases, the driving force of phase separation also increases. At the same time, the solidification rate of the polymer-rich phase is also faster.[28] Of course, the coarsening time will be shorter. Solidification and L–L phase separation are two competitive factors affecting the characteristics of the resultant pore structure.

Because the specific heat capacity of water is far larger than that of air, the cooling rate of a sample quenched in water is much faster than that in air. Therefore, the driving force of L–L phase separation for a system in water may be larger than that of a system cooled in air. The phase-separation time and coarsening time will be shorter.[49]

The average pore size of the TPX membranes quenched in water were smaller than that of the TPX membranes quenched in air. When the porosity in Table II is compared with that in Table I, one can see that the samples quenched in water had the lower porosity in the two cooling rates.

To research the influence of the smaller cooling rate on the resultant pore structure, some solutions were cooled in air slowly (cooling rate = 10°C/min). Figure 5 presents the porous structures in the TPX/DPE systems with variant TPX concentrations (20, 50, and 60%) at different cooling rates.

Figure 5(a,d,g) (20% TPX concentration, different cooling rates) presents the cellular porous structure. When the cooling rate decreased, the average pore diameter increased. When the cooling rate decreased, there was a longer time for the L–L phase separation and coarsening; therefore, the L–L phase separation was completed sufficiently, and the pore diameter was larger.

Figure 5(b,e) presents the pore structures; however, there is no obvious pore structure shown in Figure 5(h). This means that the cooling rate of 10°C/min in air was much smaller than that of the system quenched in 20°C air and water; the driving force for phase separation was too small, so no obvious pore structures were formed, as shown in Figure 5(h). When the polymer solution was quenched in 20°C water, a more porous structure was clearly present [Fig. 5(b)]. This confirmed that the cooling rate greatly influenced the resultant pore structures.

When the TPX concentration was 60%, the various cooling rates hardly influenced the pore structures. Almost no pore structures are present in Figure 5(c,f,i) because the polymer concentration of this solution was larger than that of monotectic point; only polymer crystallization and no L–L phase separation occurred, so the cooling rates did not influence the L–L phase separation.

Figure 5 shows the effect of the cooling rate on the resultant porous structures of the TPX/DPE systems with variant TPX concentrations. When the cooling rate increased in the L–L phase-separation process, the driving force of phase separation also increased. It influenced the pore structures and the average pore diameter. At the same time, when the cooling rate was too large, the coarsening time was too short and the proper pore structure could not form. When the S–L phase separation took place, the cooling rate hardly influenced the mechanism of phase separation and the resultant pore structures.

CONCLUSIONS

Porous TPX membranes with variant pore structures were formed by the TIPS method with DPE as the diluent at proper TPX concentrations and cooling rates. The concentration of the monotectic point in this system was 54 wt %.

For the TPX/DPE system, when the TPX concentration was 30%, spinodal decomposition occurred; when the concentration was 40 or 50%, nucleation–growth mechanism played an important role when the system was quenched in air. When the TPX concentration was larger than 54%, the porous structure was formed by polymer crystallization and could not form proper porous structures.

When the TPX concentration was low, quenching in water supplied a rapid cooling rate and a shorter coarsening time, which induced smaller pores. When the TPX concentration was high, the too-slow cooling rate, such as in the system cooled in air (10°C/min), did not benefit the formation of porous structures.

References

1. Vasile, C.; Seymour, R. B. Handbook of Polyolefins—Synthesis and Properties; Marcel Dekker: New York, 1993; pp 5, 486, 497, and 562.
2. Puleo, A. C.; Paul, D. R.; Wong, P. K. Polymer 1989, 30, 1357.
3. Lopez, L. C.; Wilkes, G. L.; Stricklen, P. M.; White, S. A. J Macromol Sci Rev Macromol Chem Phys 1992, 32, 301.
4. Höhne, G. W. H.; Rastogi, S.; Wunderlich, B. Polymer 2000, 41, 8869.
5. Pande, S.; Kumar, A.; Tandon, P.; Gupta, V. D. Vibr Spectrosc 2001, 26, 161.
6. Danch, A.; Osoba, W. Desalination 2004, 163, 143.
7. Samuel, E. J. J.; Mohan, S. Spectrochim Acta Part A 2004, 60, 19.
8. Rastogi, S.; Vega, J. F.; Ruth, N. J. L. V.; Terry, A. E. Polymer 2006, 47, 5555.
9. Ruan, J.; Alcazar, D.; Thierry, A.; Lotz, B. Polymer 2006, 47, 836.
10. Nagase, Y.; Kobayashi, M.; Kato, T.; Imuta, S. Eur. Pat. 573172 A1, 13 (1993).
11. Ullmann's Encyclopedia of Industrial Chemistry, 6th ed.; Wiley-VCH: Weinheim, 2001; Vol. A21, p 572.
12. Rosa, C. D.; Auriemma, F.; Borriello, A.; Corradini, P. Polymer 1995, 36, 4723.

13. Rosa, C. D.; Venditto, V.; Guerra, G.; Corradini, P. Polymer 1995, 36, 3619.
14. Rosa, C. D.; Grassi, A.; Capitani, D. Macromolecules 1998, 31, 3163.
15. Rosa, C. D.; Venditto, V.; Guerra, G.; Corradini, P. Macromolecules 1992, 25, 6938.
16. Pande, S.; Kumar, A.; Tandon, P.; Gupta, V. D. Vibr Spectrosc 2001, 26, 161.
17. Drioli, E.; Romano, M. Ind Eng Chem Res 2001, 40, 1277.
18. Wang, D. M.; Lin, F. C.; Wu, T. T.; Lai, J. Y. J Membr Sci 1997, 123, 35.
19. Twarowska-Schmidt, K.; Wtochowicz, A. J Membr Sci 1997, 137, 55.
20. Wang, D. M.; Lin, F. C.; Chiang, J. C.; Lai, J. Y. J Membr Sci 1998, 141, 1.
21. Wang, Y. C.; Li, C. L.; Chang, P. F.; Fan, S. C.; Lee, K. R.; Lai, J. Y. J Membr Sci 2002, 208, 3.
22. Shin, S. C.; Yoon, M. K. Int J Pharm 2002, 232, 131.
23. Danch, A.; Osoba, W. Desalination 2004, 163, 143.
24. Lee, K. H.; Givens, S.; Chase, D. B.; Rabolt, J. F. Polymer 2006, 47, 8013.
25. Castro, A. J. U.S. Pat. 4,247,498 (1981).
26. Rowlands, A. S.; Lim, S. A.; Martin, D.; Cooper-White, J. J. Biomaterials 2007, 28, 2109.
27. Ding, H.; Zhang, Q.; Tian, Y.; Shi, Q.; Liu, B. J Appl Polym Sci 2007, 104, 1523.
28. Ding, H.; Zeng, Y.; Meng, X.; Tian, Y.; Shi, Y.; Jiao, Q.; Zhang, S. J Appl Polym Sci 2006, 102, 2959.
29. Hua, F. J.; Kim, G. E.; Lee, J. D.; Son, Y. K.; Lee, D. S. J Biomed Mater Res Appl Biomater 2002, 63, 161.
30. Hua, F. J.; Park, T. G.; Lee, D. S. Polymer 2003, 44, 1911.
31. Shin, K. C.; Kim, B. S.; Kim, J. H.; Park, T. G.; Nam, J. D.; Lee, D. S. Polymer 2005, 46, 3801.
32. Kim, D. H.; Bae, E. H.; Kwon, I. C.; Pal, R. R.; Nam, J. D.; Lee, D. S. Biomaterials 2004, 25, 2319.
33. Matsuyama, H.; Berghmans, S.; Batarseh, M. T.; Lloyd, D. R. J Membr Sci 1998, 142, 27.
34. Matsuyama, H.; Iwatani, T.; Kitamura, Y.; Tearamoto, M. J Appl Polym Sci 2001, 79, 2456.
35. Matsuyama, H.; Iwatani, T.; Kitamura, Y.; Tearamoto, M.; Sugoh, N. J Appl Polym Sci 2001, 79, 2449.
36. Matsuyama, H.; Kobayashi, K.; Maki, T.; Tearamoto, M. J Appl Polym Sci 2001, 82, 2583.
37. Matsuyama, H.; Kim, M.; Lloyd, D. R. J Membr Sci 2002, 204, 413.
38. Shang, M. X.; Matsuyama, H.; Tearamoto, M.; Lloyd, D. R.; Kubota, N. Polymer 2003, 44, 7441.
39. Shang, M. X.; Matsuyama, H.; Maki, T.; Tearamoto, M.; Lloyd, D. R. J Appl Polym Sci 2003, 87, 853.
40. Matsuyama, H.; Ohga, K.; Maki, T.; Tearamoto, M.; Nakatsuka, S. J Appl Polym Sci 2003, 89, 3951.
41. Lloyd, D. R.; Kim, S. S.; Kinzer, K. E. J Membr Sci 1991, 64, 1.
42. Kim, S. S.; Lloyd, D. R. J Membr Sci 1991, 64, 13.
43. Lim, G. B. A.; Kim, S. S.; Ye, Q.; Wang, Y. F.; Lloyd, D. R. J Membr Sci 1991, 64, 31.
44. Kim, S. S.; Lim, G. B. A.; Alwattari, A. A.; Wang, Y. F.; Lloyd, D. R. J Membr Sci 1991, 64, 41.
45. Alwattari, A. A.; Lloyd, D. R. J Membr Sci 1991, 64, 55.
46. McGuire, K. S.; Lloyd, D. R.; Lim, G. B. A. J Membr Sci 1993, 79, 27.
47. Graham, P. D.; McHugh, A. J. Macromolecules 1998, 31, 2565.
48. Hiatt, W. C.; Vitzhum, G. H.; Wagener, K. B.; Gerlach, K.; Josefiak, C. Materials Science of Synthetic Membranes; ACS Symposium Series 269; American Chemical Society: Washington, DC, 1985; p 299.
49. Zhang, J.; Luo, F.; Wang, X.-L.; Chen, J.-F.; Xu, Z.-Z. Acta Polym Sinica 2003, 2, 241.